Supporting Information

Architecture Engineering Toward Highly Active Palladium Integrated Titanium Dioxide Yolk-Double-Shell Nanoreactor for Catalytic Applications

Baocang Liu,[a,b] Qin Wang,[a,c] Shengli Yu,[a] Peng Jing,[a] Lixia Liu,[a] Gangran Xu,[a] and Jun Zhang*[a,b,c]

[a] College of Chemistry and Chemical Engineering, Inner Mongolia University, Hohhot 010021, P. R. China

[b] College of Life Science, Inner Mongolia University, Hohhot 010021, P. R. China

[c] Inner Mongolia Key Lab of Nanoscience and Nanotechnology, Hohhot 010021, P. R. China

Corresponding Author: J. Zhang, cejzhang@imu.edu.cn

Experimental

1. Synthesis of SiO_2/Pd (SOL-IMP) and SiO_2@TiO_2/Pd (SOL-IMP) catalysts.

Typically， $PdCl_2$ solution (1 g/L, 4 mL) and PVA solution (1 wt%, 0.31 mL) were diluted to 100 mL with deionized water under vigorous stirring. After 30 min, $NaBH_4$ solution (0.1 mol/L, 1.1 mL) was injected into the above solution, and a dark-brown solution was obtained, which indicated that the Pd colloids were formed. After another 30 min, 0.2 g of amino modified SiO_2 or SiO_2@TiO_2 sphere was added immediately. After stirring for 4 h, the Pd colloids were completely absorbed, as indicated by the discoloration of the solution. The SiO_2/Pd(SOL-IMP) and SiO_2@TiO_2/Pd(SOL-IMP) were collected by centrifugation, and washed three times with deionized water. Finally, SiO_2/Pd(SOL-IMP) and SiO_2@TiO_2/Pd(SOL-IMP) were calcinated at 600 ^oC for 3h, and reduced in a hydrogen atmosphere at 300°C for 2 h. Thus, the finally SiO_2/Pd(SOL-IMP) and SiO_2@TiO_2/Pd(SOL-IMP) catalysts were obtained.

2. Synthesis of SiO_2/Pd (ION-IMP) and SiO_2@TiO_2/Pd (ION-IMP) catalysts.

In a typical synthesis, amino modified SiO_2 or SiO_2@TiO_2 sphere (0.2 g) was added into 4 mL of $PdCl_2$ solution (1 g/L), and the mixture solution was diluted to 100 mL with deionized water. After stirring 12 h, the products were collected by centrifugation, washed five times with deionized water. Then, the obtained SiO_2/Pd^{2+} and SiO_2@TiO_2/Pd^{2+} were calcinated at 600 ^oC for 3h, following reduction under H_2 atmosphere at 300°C for 2 h to achieve the finally SiO_2/Pd(ION-IMP) and SiO_2@TiO_2/Pd(ION-IMP) catalysts.

3. Synthesis of Pd@SiO_2 catalyst.

First, 4 mL of Pd Sol (1g/L) was added into a beaker charged with absolute ethanol (66 mL), and ammonia solution (3.4 mL) under stirring for 30 min. Afterward, TEOS (0.4 mL) was added, and the reaction was carried out at room temperature for 24 h under continuous magnetic stirring. The Pd@SiO_2 spheres were obtained by centrifugation and washed three times with deionized water and absolute ethanol. Then, the obtained Pd@SiO_2 were calcinated at 600 ^oC for 3h, following reduction under H_2 atmosphere at 300°C for 2 h to achieve the finally Pd@SiO_2 catalysts.

Discussion

The possible mechanism of yolk-double-shell Pd@TiO_2/Pd@TiO_2 for improved catalytic performance

As illustrated in Scheme S3, the higher catalytic activity of the yolk-double-shell Pd@TiO_2/Pd@TiO_2 catalyst may have several causes. First, the yolk-double-shell configuration has two independent compartments (the interlayer chamber between the double TiO_2 shells and central cavity), which can be used as a nanoreactor. Because of the confinement effect in the microenvironments, it may be more effective than other traditional single-shell hollow nanoreactors for enriching reactants. The high concentration of reactants in the nanoreactor may accelerate the catalytic reaction,[1] leading to higher catalytic activity. Second, PNPs are highly dispersed onto both the external and internal surfaces of the inner TiO_2 shell, enhancing the synergistic effect between PNPs and TiO_2 shells. This can be proven

by the fact that the double-shell @TiO_2@Pd@TiO_2 catalyst with PNPs encapsulated in the interlayer space has low catalytic activity for bromobenzene, and the conversion rate is only 8.9% after 60 min. This may be due to the lower interaction of PNPs with TiO_2 shells, leading to a weak synergistic effect and low catalytic activity. In addition, as PNPs are well dispersed on both surfaces of the inner TiO_2 shell, increasing PNPs active sites in contact with the reactants, which improves the catalytic performance.[2] Third, because the inner TiO_2 shell is composed of TiO_2 nanocrystals with less crystallization, a large number of –OH groups rooted from the hydrolysis of tetrabutyl orthotitanate (TBOT) exist on the surface of the TiO_2 shell. It is well known that the oxidative addition (Step I in Scheme S3) is the rate-determining step during the Suzuki-Miyaura coupling reaction. The synergistic effect between the PNPs and –OH groups on the surface inner TiO_2 shell will speed up the reaction by increasing the reaction rate of step I.[3] The products are finally generated after transmetalation (Step II and III) and reductive climination (Step IV). Fourth, the rational design of the yolk-double-shell Pd@TiO_2/Pd@TiO_2 architecture may improve catalytic activity, since the inner TiO_2 shell can prevent PNPs from growing larger during preparation, and the outer TiO_2 shell prevents the deletion of PNPs and creates an interlayer chamber connecting with the central cavity to form nanoreactors. Such design may favor improved catalytic efficiency. Finally, the mesoporous TiO_2 shells favor the easy diffusion of reactants and products, which is beneficial for heterogeneous catalysis.

Table S1. Comparison of catalytic performance of the obtained double-shell @TiO_2/Pd@TiO_2 (ION-IMP) catalysts with the previously reported Pd-based catalysts in recent years for Suzuki–Miyaura coupling reactions of iodobenzene and phenylboronic acid.

Catalyst	Temp. [°C]	Pd [mol]	D_{Pd} [nm]	Solvent	Time [h]	Conversion [%]	Ref.
@Pd/TiO_2/Pd@TiO_2	80	0.054	4, 20	EtOH	0.16	99	This work
Pd/Nf-G	80	0.3	6	EtOH/H_2O	1	94	[4]
Pd/polymer	100	0.5	50	DMF/H_2O	12	100	[5]
Fe_3O_4@SiO_2@mSiO_2-Pd	80	0.075	4-10	Isopropanol	6	98	[6]
Pd/SBA-16	80	0.5	—	EtOH	2	99	[7]
HMMS–NH_2–Pd	70	0.6	9	EtOH	0.5	99	[8]
MWNT/Pd	70	2	1.1	MeOH	4	100	[9]
Pd/Fe_3O_4	86	0.2	5	EtOH/H_2O	0.5	97	[10]
Pd/Fe_3O_4@C	60	1	10	EtOH/H_2O	2	99	[11]
Pd/MFC	78	0.308	15	EtOH	1	100	[12]
Pd/MIL-53(Al)-NH_2	40	0.5	3.1	EtOH/H_2O	0.5	94	[13]
LDH-Pd(0)	80	0.3	3.5	Dioxane/Water	10	96	[14]
Pd/modified silica Gel	110	1	5	DMF	4	94	[15]
Pd@peptide	25	1.5	12-14	H_2O	4	99	[16]
Pd/NF300	80	0.08	3-5	H_2O	4	97	[17]
IL-PdNPs	100	1	6	H_2O	1	98	[18]
Pd-Fe_3O_4	reflux	1	9	DME/H_2O	24	99	[19]
Pd-graphene	100	1.1	4	H_2O	0.12	100	[20]
Pd/MCPCC	80	0.1	18-30	DMF	0.67	96	[21]
Fe@Fe_xO_y/Pd	25	0.5	3-45	EtOH/H_2O	2	98	[22]
Pd/CD	60	0.01	—	H_2O	24	100	[23]
Pd(0)-MCM-41	80	0.5	2-7	EtOH/H_2O	20	100	[24]
PS-co-PVP-Pd	90	0.25	3.9	NEt_3	3	99	[25]
Pd nanocrystals	85	1.6	300	EtOH/H_2O	4	92	[26]
Pd/CNTPs	reflux	0.13	2-5	EtOH	0.5	99	[27]
NanoPd-MWNTs	110	0.25	2-4	DMF	2	100	[28]

Table S2. Suzuki–Miyaura coupling reactions of aryl halides on double-shell @TiO_2/Pd@TiO_2 (SOL-IMP) catalysts[a]

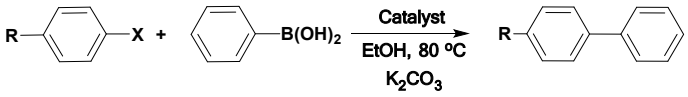

Entry	X	R	Pd [mol%]	Reaction Time [min]	Conversion [%]	TOF [(h^{-1})]
1	I	H	0.056	20	99.5	5330
2	I	-NO_3	0.056	20	99.5	5330
3	I	-OH	0.056	20	92.7	4966
4	I	-COOH	0.056	20	93.4	5003
5	I	-F	0.056	20	99.1	5309
6	I	-$COCH_3$	0.056	25	93.6	4011
7	I	-CH_3	0.056	25	91.2	3908
8	I	-NH_2	0.056	30	78.1	2789
9	I	-OCH_3	0.056	30	74.3	2653

Table S3. Actual Pd content loaded on different catalysts and their corresponding turnover frequencies (TOF) for 4-nitrophenol reduction reactions.

Catalysts	Actual content of Pd [wt%]	TOF (h^{-1})[a)]
Pd@TiO_2/Pd@TiO_2 (ION-IMP)	0.12	801
@TiO_2/Pd@TiO_2 (SOL-IMP)	0.15	236
@TiO_2@Pd@TiO_2 (SOL-IMP)	0.96	24
@TiO_2/Pd (ION-IMP)	0.76	38
@TiO_2/Pd (SOL-IMP)	0.88	20

[a] TOF is defined as the moles of reduced 4-nitrophenol molecules per mole of Pd atom in catalyst per hour.

Table S4. Actual and theoretical hydrogen consumptions of the reduction peak in different catalysts.

Catalysts	Actually hydrogen consumption[a] [$\mu mol \cdot g^{-1}_{Cat.}$]	Theoretical hydrogen consumption [$\mu mol \cdot g^{-1}_{Cat.}$]
PdO@SiO_2	9.61	9.25
SiO_2/PdO (ION-IMP)	8.27	7.98
SiO_2@TiO_2/PdO (ION-IMP),	15.5	6.56
@PdO/TiO_2/PdO@TiO_2 (ION-IMP)	5.17	1.13

[a]The amount of H_2 uptake during the reduction was measured by a thermal conductivity detector (TCD), which was calibrated by the quantitative reduction of CuO to the metallic copper.

Table S5. Suzuki-Miyaura coupling reaction of halogeno benzene over different catalysts.[a]

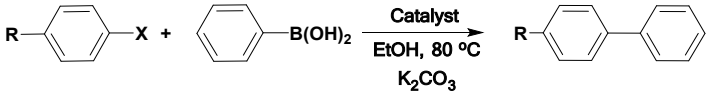

Catalyst	X	R	Reaction [min]	Pd [mol%]	Conversion [%]	TOF [h^{-1}]	D_{Pd} [nm]	Actual content of Pd [wt%]
SiO_2/Pd (SOL-IMP)	I	H	20	0.35	97.3	836	8-10	0.91
SiO_2/Pd (ION-IMP)	I	H	20	0.32	97.6	917	10-12	0.85
SiO_2@TiO_2/Pd (SOL-IMP)	I	H	10	0.29	99.1	2055	10-20	0.71
SiO_2@TiO_2/Pd (ION-IMP)	I	H	10	0.27	99.2	2209	12-20	0.70
Pd@SiO_2	I	H	20	0.37	99	805	15	0.98
Pd sol	I	H	10	0.30	99.5	2053	3-5	100
SiO_2/Pd (SOL-IMP)	Br	H	60	0.35	9.5	27	8-10	0.91
SiO_2/Pd (ION-IMP)	Br	H	60	0.32	10.3	32	10-12	0.85
SiO_2@TiO_2/Pd (SOL-IMP)	Br	H	60	0.29	48.3	167	10-20	0.71
SiO_2@TiO_2/Pd (ION-IMP)	Br	H	60	0.27	48.8	181	12-20	0.70
Pd@SiO_2	Br	H	60	0.37	11.2	30	15	0.98
Pd sol	Br	H	60	0.30	40	134	3-5	100

[a]Reaction conditions: 80°C ethanol (10 mL), iodobenzene or bromobenzene (0.5 mmol), phenylboronic acid (1 mmol), K_2CO_3 (1 mmol), and catalyst (20 mg).
[b]Determined by HPLC using pentamethylbenzene as internal standard.
[c]TOF is calculated by moles of product per molar Pd per hour.

Table S6. Actual Pd loading content on different catalysts and their corresponding turnover frequencies (TOF) for 4-nitrophenol reduction reaction.

Catalysts	Actual content of Pd [wt.%]	TOF (h^{-1})[a]
$Pd@TiO_2/Pd@TiO_2$ (ION-IMP)	0.12	801
$@TiO_2/Pd@TiO_2$ (SOL-IMP)	0.15	236
$@TiO_2@Pd@TiO_2$ (SOL-IMP)	0.96	24
$@TiO_2/Pd$ (ION-IMP)	0.76	38
$@TiO_2/Pd$ (SOL-IMP)	0.88	20
$Pd@SiO_2$	0.98	27
SiO_2/Pd (SOL-IMP)	0.91	15
SiO_2/Pd (ION-IMP)	0.85	18
$SiO_2@TiO_2/Pd$ (SOL-IMP)	0.75	30
$SiO_2@TiO_2/Pd$ (ION-IMP)	0.70	25
Pd sol	-	170

[a]TOF is defined as the moles of reduced 4-nitrophenol molecules per mole of Pd atom in catalyst per hour.

Table S7. Suzuki-Miyaura coupling reaction of bromobenzene over double-shell $Pd@TiO_2/Pd@TiO_2$ catalysts with different sizes of Pd nanoparticles at 4, 6, and 11 nm.

Catalyst	X	R	Reaction [min]	Pd [mol%]	D_{Pd} [nm]	Conversion [%]	TOF [h^{-1}]	Actual content of Pd [wt%]
$Pd@TiO_2/Pd@TiO_2$	Br	H	60	0.045	4	72	1600	0.12
$Pd@TiO_2/Pd@TiO_2$	Br	H	60	0.034	6	42	1244	0.09
$Pd@TiO_2/Pd@TiO_2$	Br	H	60	0.034	11	24	711	0.09

[a]Reaction conditions: 80°C ethanol (10 mL), bromobenzene (0.5 mmol), phenylboronic acid (1 mmol), K_2CO_3 (1 mmol), and catalyst (20 mg).
[b]Determined by HPLC using pentamethylbenzene as internal standard.
[c]TOF is calculated by moles of product per molar Pd per hour.

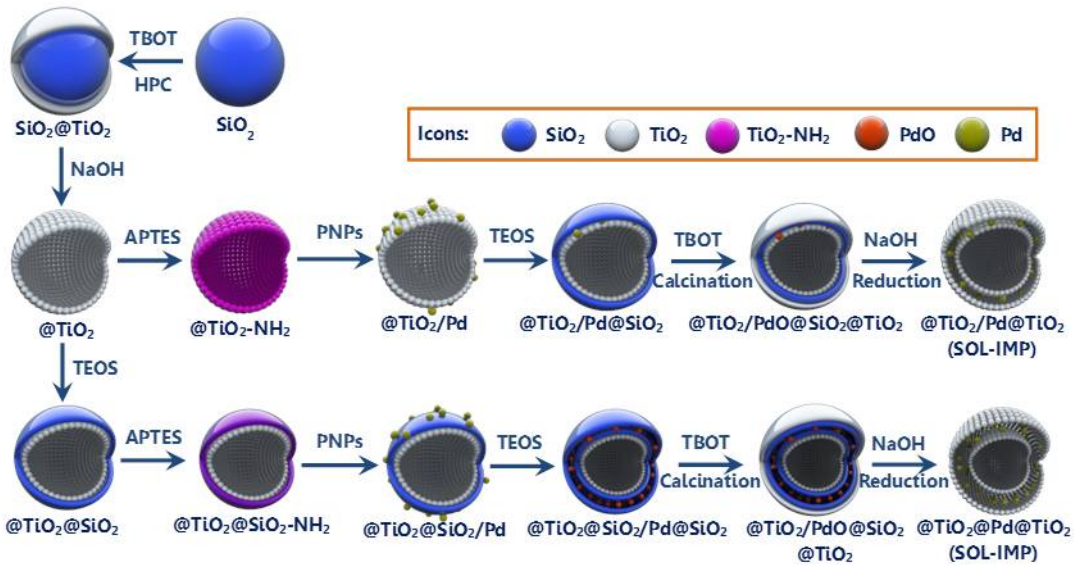

Scheme S1. Schematic diagram illustrating the synthesis of double-shell @TiO_2/Pd@TiO_2 architecture with PNPs loaded on the external surface of the inner TiO_2 shell and double-shell @TiO_2@Pd@TiO_2 architecture with PNPs dispersed in the interlayer space of double TiO_2 shells via a Pd sol impregnation process.

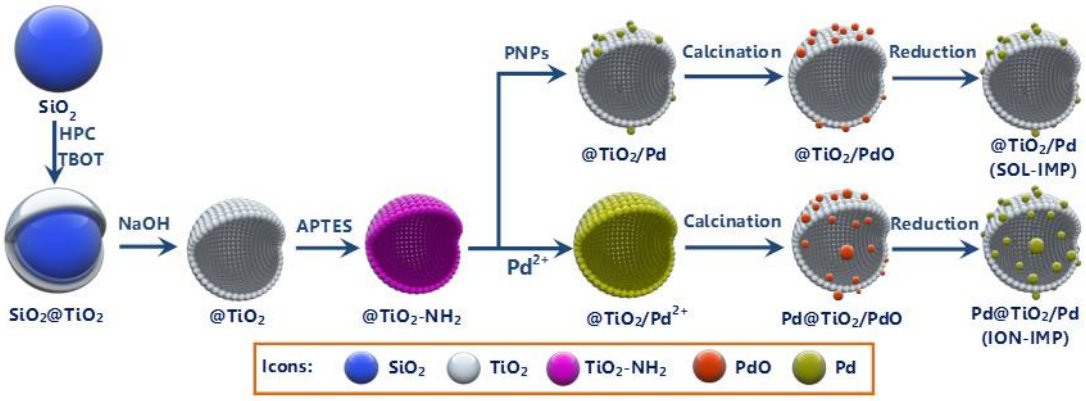

Scheme S2. Schematic diagram illustrating the synthesis of yolk-single-shell Pd@TiO_2/Pd with yolk-type PNPs residing inside the central cavity and PNPs loaded on the external surface of the TiO_2 shell via a Pd^{2+} ion-disffusion impregnation process and single-shell @TiO_2/Pd architectures with PNPs loaded on the external surface of the TiO_2 shell via a Pd sol impregnation process.

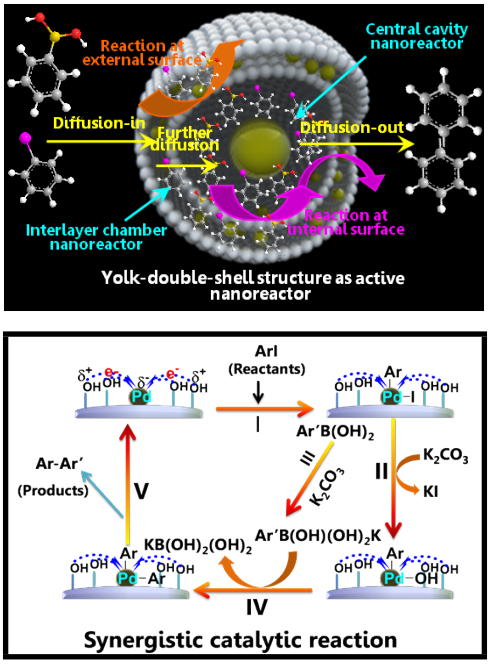

Scheme S3. Schematic illustration showing the improvement of synergistic catalytic effect (upper) and the catalytic process of Suzuki-Miyaura coupling reaction (lower) on a yolk-double-shell Pd@TiO_2/Pd@TiO_2 nanoreactor.

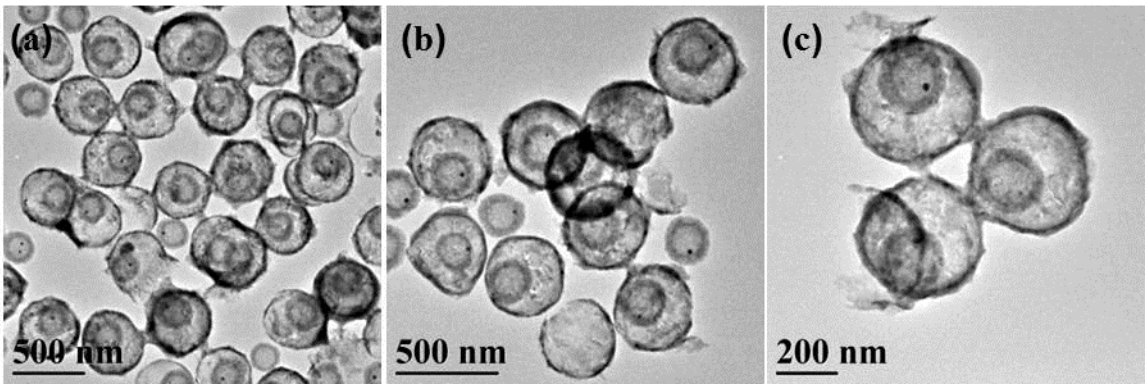

Fig. S1. (a-c) Low magnification TEM images showing yolk-double-shell Pd@TiO_2/Pd@TiO_2 architectures with yolk-type PNPs residing in the double-shell TiO_2 cavity and ultrafine PNPs loading on both external and internal surfaces of the inner TiO_2 shell prepared via a Pd^{2+} ion-diffusion impregnation method.

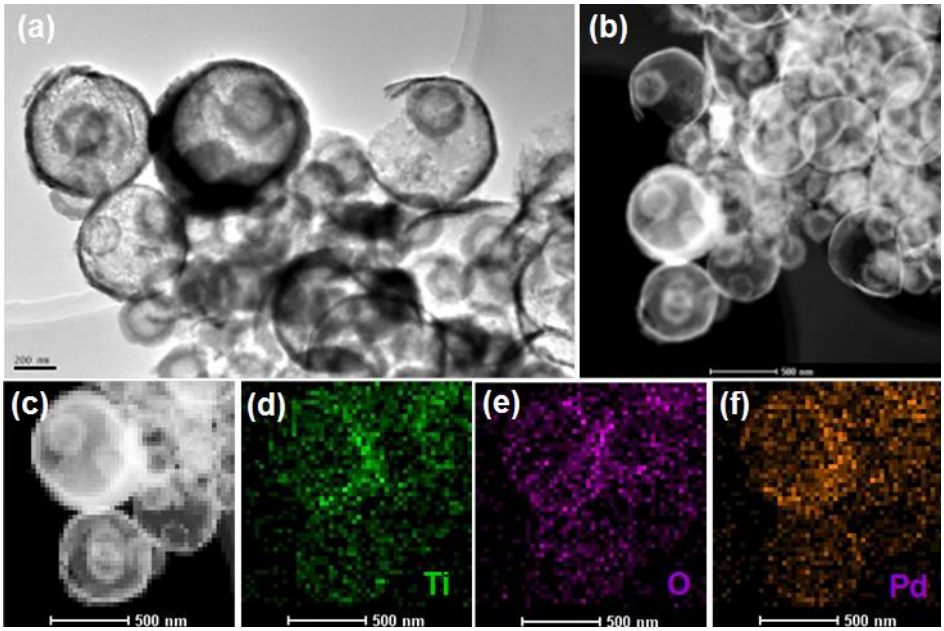

Fig. S2 (a) TEM and (b and c) HADDF-STEM images of yolk-double-shell Pd@TiO_2/Pd@TiO_2 architecture prepared by enlarging the dosage of all reactants five times, and (d-f) EDX elemental mapping of Ti, O, and Pd in yolk-double-shell Pd@TiO_2/Pd@TiO_2 architecture.

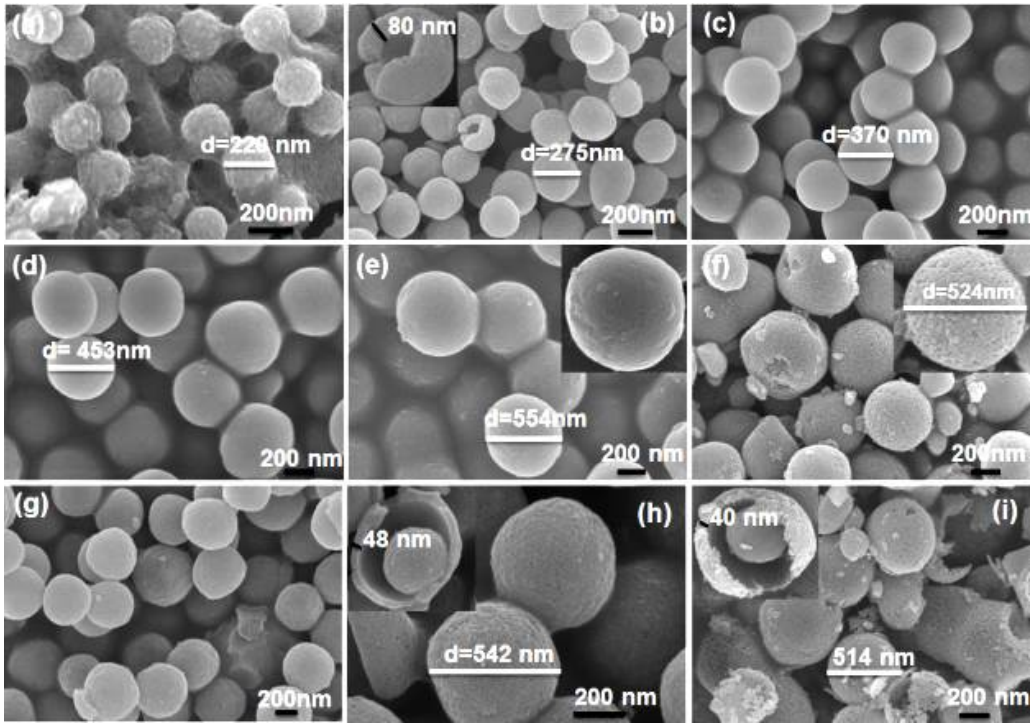

Fig. S3. The SEM images monitoring the formation of double-shell @TiO_2@Pd@TiO_2 architecture with PNPs loaded in the interlayer space of the double TiO_2 shells prepared via a Pd sol impregnation method. (a) SiO_2@TiO_2, (b) @TiO_2, (c) @TiO_2@SiO_2/Pd, (d) @TiO_2@SiO_2/Pd@SiO_2, (e) @TiO_2@SiO_2/Pd@SiO_2@TiO_2 (before calcination), (f) @TiO_2@SiO_2/Pd@SiO_2@TiO_2 (after calcination), (g) and (h) @TiO_2@Pd@TiO_2 (before calcination), and (i) @TiO_2@Pd@TiO_2 (after calcination). The insets in b, e, f, h, and i show the magnified FE-SEM images for a broken or an individual sphere.

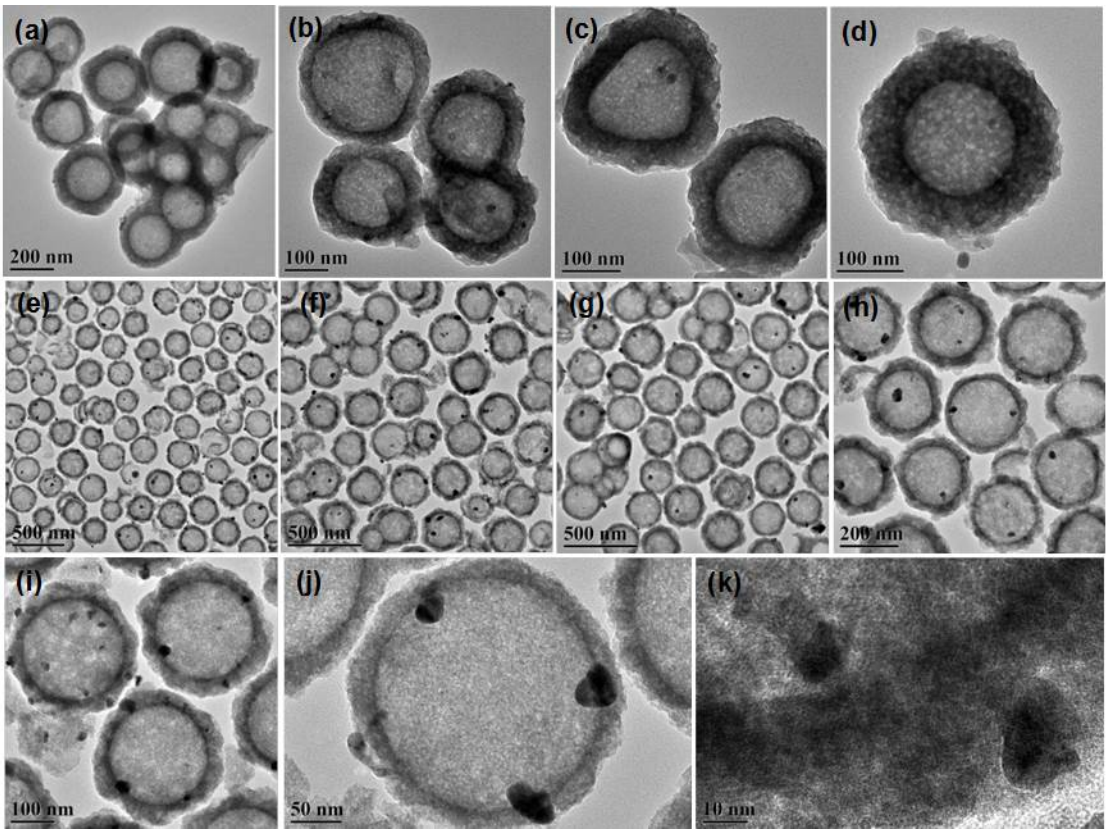

Fig. S4. TEM images illustrating the formation of (a-d) single-shell @TiO_2/Pd architecture with PNPs loaded on the external surface of the inner TiO_2 shell prepared via a Pd sol impregnation method, and (e-k) yolk-single-shell Pd@TiO_2/Pd architectures with yolk-type PNPs residing inside the central cavity and PNPs loaded on the external surface of the TiO_2 shell prepared via a Pd^{2+} ion-diffusion method.

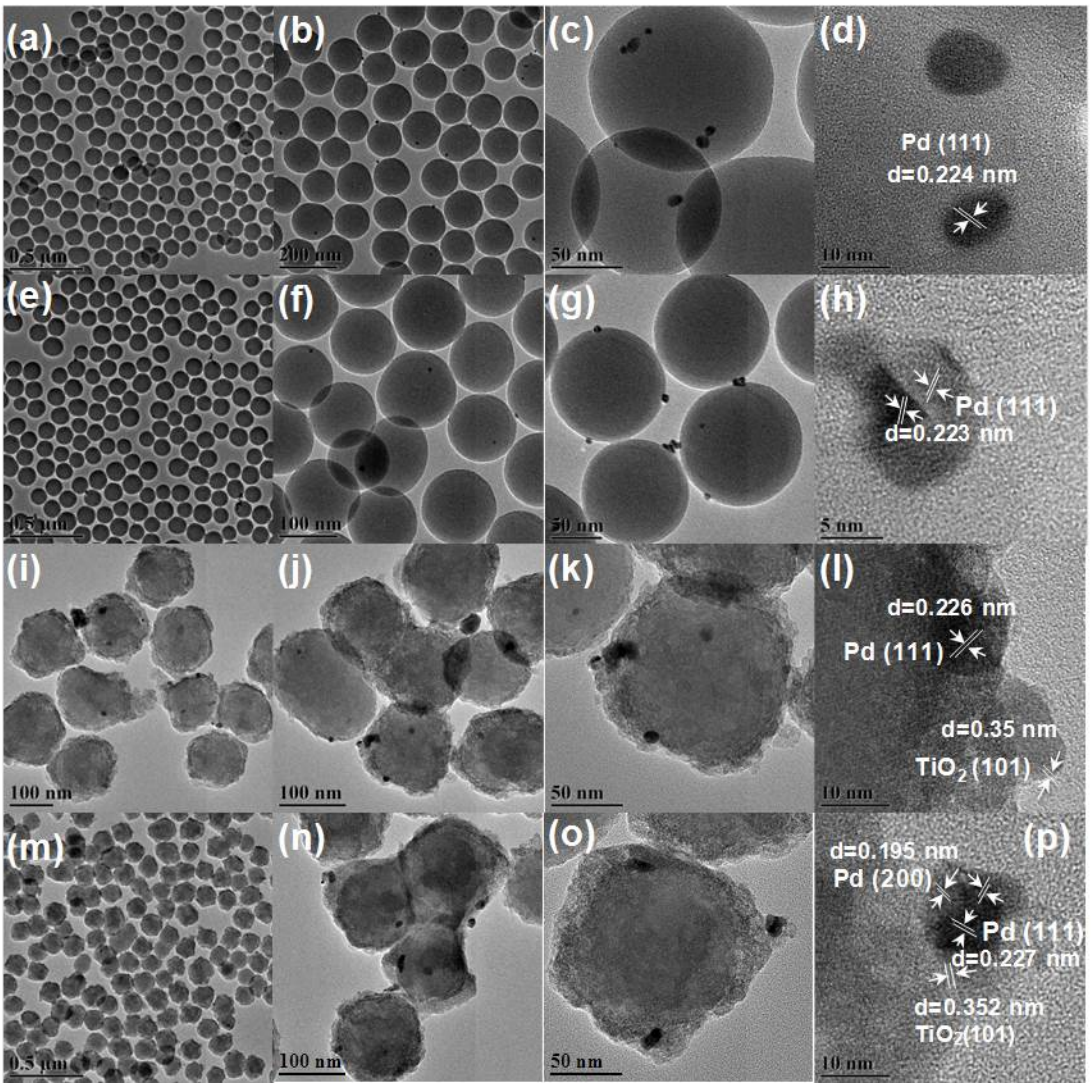

Fig. S5. TEM images of (a-d) SiO_2/Pd (SOL-IMP), (e-h) SiO_2/Pd (ION-IMP), (i-l) SiO_2@TiO_2/Pd (SOL-IMP), and (m-p) SiO_2@TiO_2/Pd (ION-IMP) catalysts.

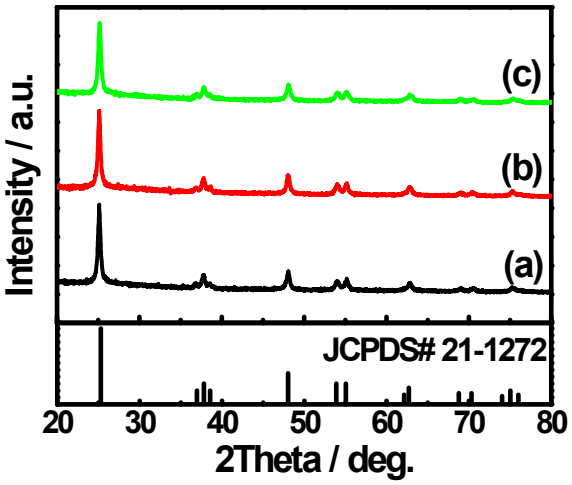

Fig. S6. XRD patterns of (a) TiO_2@Pd@TiO_2, (b) @TiO_2/Pd@TiO_2, and (c) Pd@TiO_2/Pd@TiO_2 architectures after calcination.

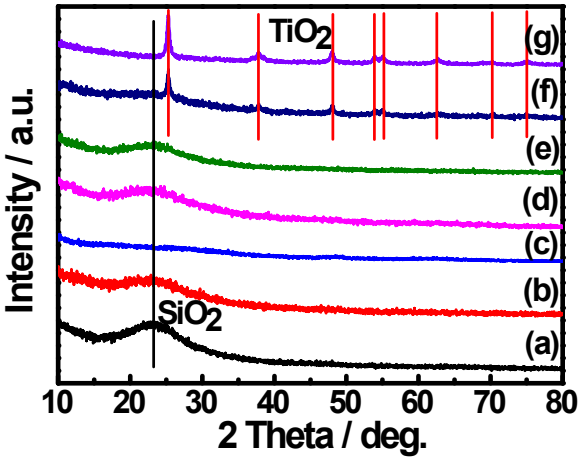

Fig. S7. XRD patterns monitoring the formation of double-shell @TiO_2@Pd@TiO_2 architectures. (a) SiO_2, (b) SiO_2@TiO_2, (c) @TiO_2, (d) @TiO_2/Pd@SiO_2 (e) @TiO_2@SiO_2/Pd@SiO_2@TiO_2 (before calcination), (f) @TiO_2@SiO_2/Pd@SiO_2@TiO_2 (after calcination), and (g) @TiO_2@Pd@TiO_2 (after calcination).

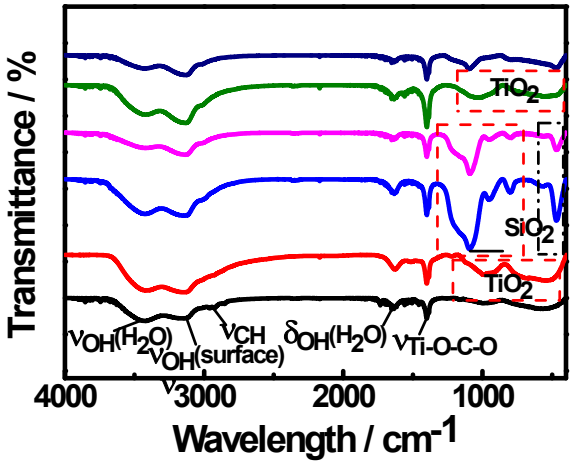

Fig. S8. FT-IR spectra monitoring the formation of yolk-double-shell $Pd@TiO_2/Pd@TiO_2$ architectures (a) $@TiO_2$, (b) $@TiO_2$-NH_2/Pd, (c) $@TiO_2/Pd@SiO_2$, (d) $@TiO_2/Pd@SiO_2@TiO_2$, (e) $Pd@TiO_2/Pd@TiO_2$ (before calcination), and (f) $Pd@TiO_2/Pd@TiO_2$ (after calcination).

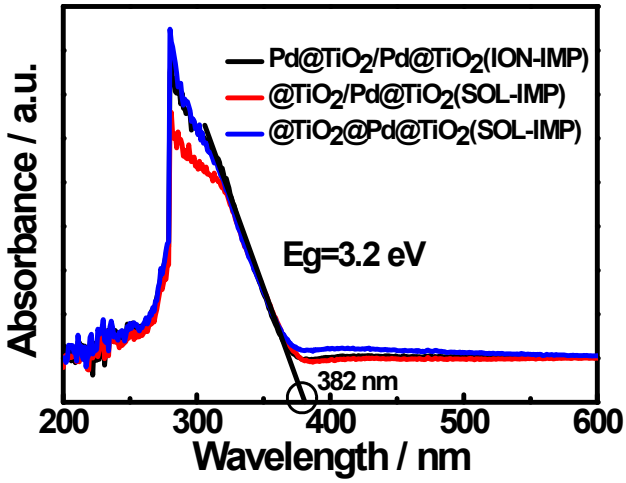

Fig. S9. UV-DRS spectra of $Pd@TiO_2/Pd@TiO_2$, $@TiO_2/Pd@TiO_2$, and $TiO_2@Pd@TiO_2$ architectures after calcination.

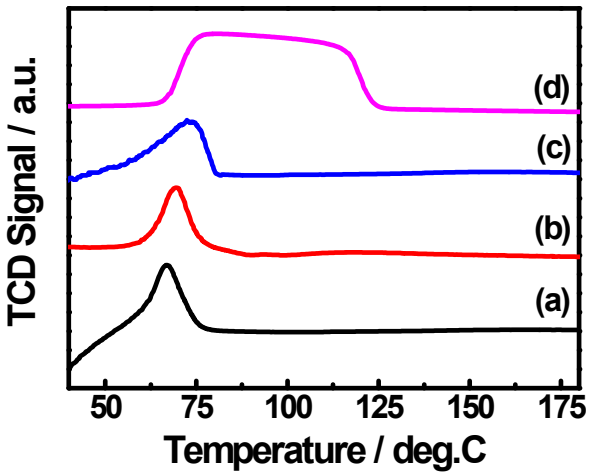

Fig. S10. TPR profiles of (a) yolk-double-shell PdO@TiO_2/PdO@TiO_2, (b) double-shell @TiO_2/PdO@TiO_2, (c) @TiO_2@PdO@TiO_2 architectures after calcination, and (d) pure PdO.

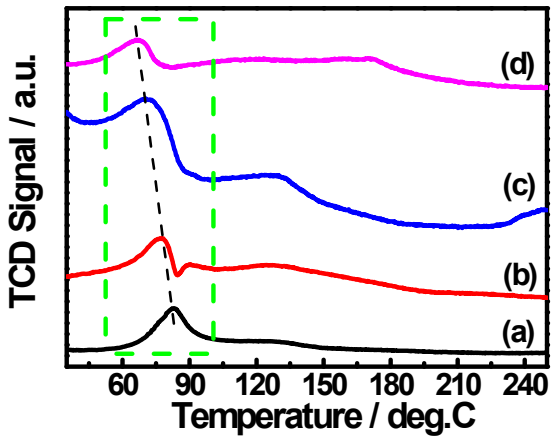

Fig. S11. H_2-TPR profiles of (a) PdO@SiO_2, (b) SiO_2/PdO (ION-IMP), (c) SiO_2@TiO_2/PdO (ION-IMP), and (d) PdO@TiO_2/PdO@ TiO_2 (ION-IMP) catalysts.

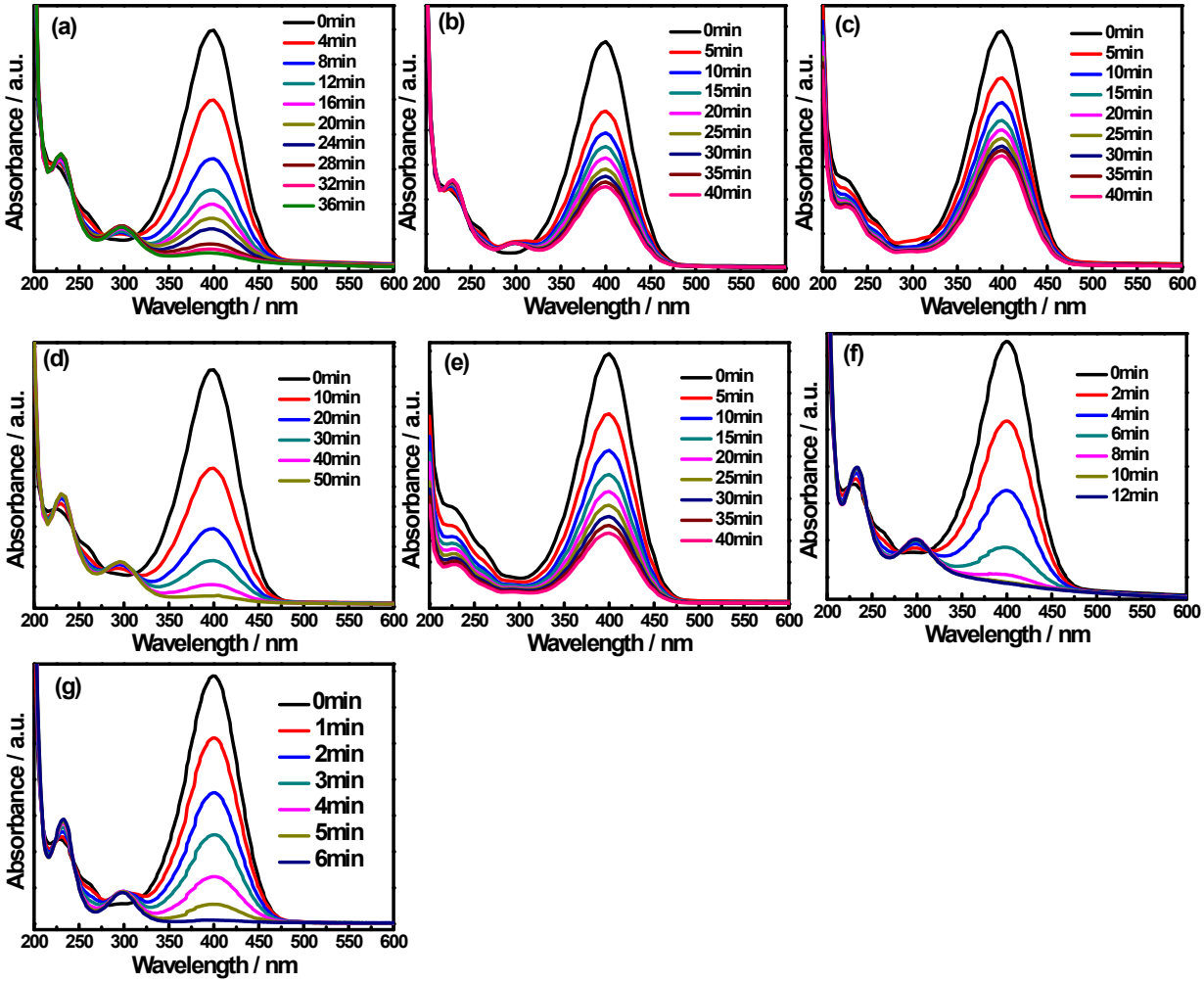

Fig. S12. UV-vis spectra indicating the reduction of 4-NP to 4-AP on (a)Pd@SiO_2, (b) SiO_2 Pd/ (SOL-IMP), (c) SiO_2/Pd (ION-IMP), (d) SiO_2@TiO_2/Pd (SOL-IMP), (e) SiO_2@TiO_2/Pd (ION-IMP),(f) Pd@TiO_2/Pd@TiO_2 (ION-IMP), and (g) Pd sol catalysts.

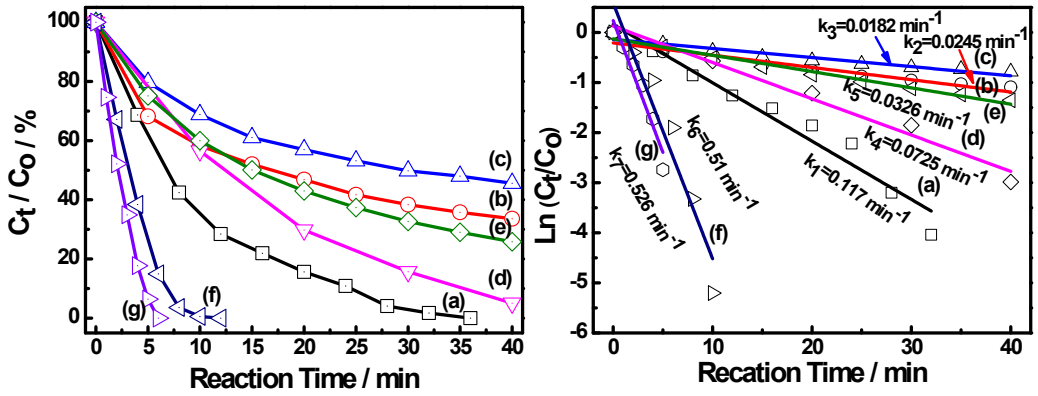

Fig. S13. (A) Catalytic tests of reduction rate for the reduction of 4-nitrophenol on (a) Pd@SiO2, (b) SiO_2/Pd (SOL-IMP), (c) SiO_2/Pd (ION-IMP), (d) SiO_2@TiO_2/Pd (SOL-IMP), (e) SiO_2@TiO_2/Pd/(ION-IMP), (f) Pd@TiO_2/Pd@TiO_2 (ION-IMP), and (g) Pd sol, (B) Plot of ln(C_t/C_0) against the reaction time of on (a) Pd@SiO_2, (b) SiO_2/Pd (SOL-IMP), (c) SiO_2/Pd (ION-IMP), (d) SiO_2@TiO_2/Pd (SOL-IMP), (e) SiO_2@TiO_2/Pd (ION-IMP), (f) Pd@TiO_2/Pd@TiO_2 (ION-IMP), and (g) Pd sol catalysts

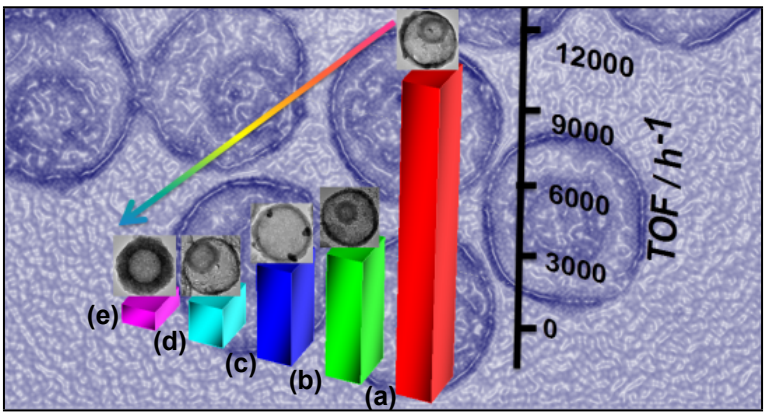

Fig. S14. The TOFs of (a) yolk-double-shell Pd@TiO_2/Pd@TiO_2, (b) double-shell @TiO_2/Pd@TiO_2, (c) yolk-single-shell Pd@TiO_2/Pd, (d) single-shell @TiO_2/Pd, and (e) double-shell @TiO_2@Pd@TiO_2 architectures.

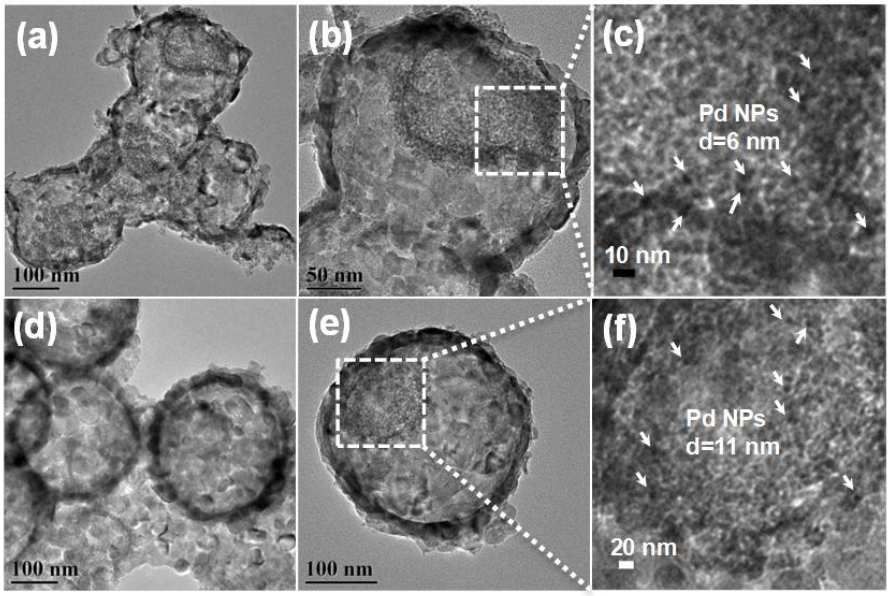

Fig S15. TEM images of double-shell Pd@TiO_2/Pd@TiO_2 catalysts with different sizes of Pd nanoparticles at (a-c) 6 nm, (d-f) 11 nm.

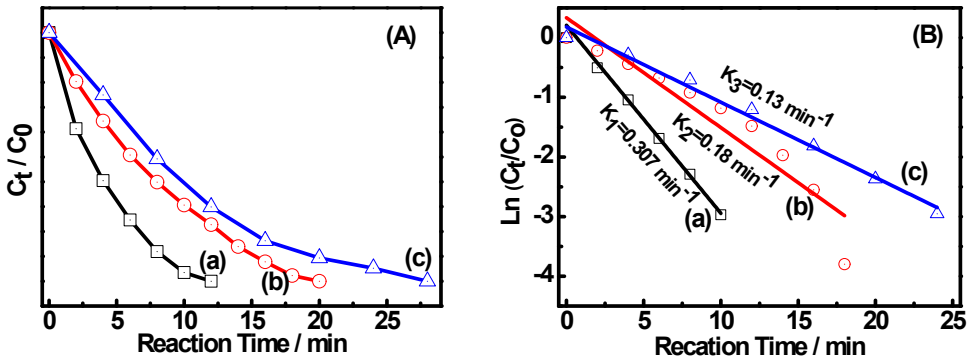

Fig S16. (A) Catalytic reduction rate of double-shell Pd@TiO_2/Pd@TiO_2 catalysts with different sizes of Pd nanoparticles at (a) 4 nm, (b) 6 nm, and (c) for the reduction of 4-NP to 4-AP; (B) Plot of ln(C_t/C_0) against the reaction time of double-shell Pd@TiO_2/Pd@TiO_2 catalysts with different sizes of Pd nanoparticles at (a) 4 nm, (b) 6 nm, and (c) 11 nm.

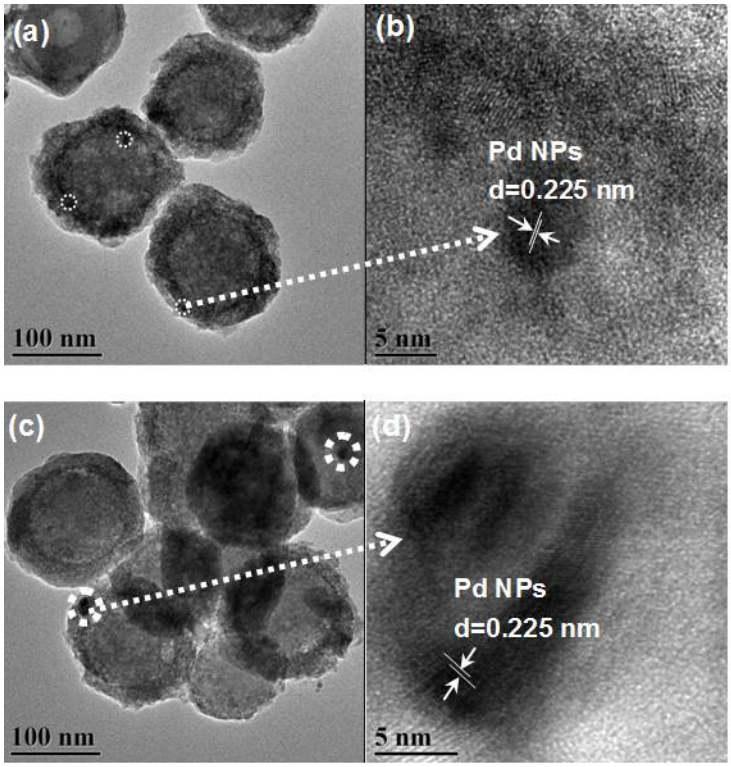

Fig. S17. (a and b) TEM images of SiO_2@TiO_2/Pd structure (fresh) and (c and d) SiO_2@TiO_2/Pd catalysts (after fourth cycle testing).

References

[1] [1] Y. Yang, X. Liu, X. B. Li, J. Zhao, S. Y. Bai, J. Liu and Q. H. Yang, *Angew. Chem. Int. Ed*., 2012, **51**, 9164.

[2] M. Cargnello, J. J. Delgado Jaen, J. C. Hernandez Garrido, K. Bakhmutsky, T. Montini, J. J. Calvino Gamez, R. J. Gorte and P. Fornasiero, *Science,* 2012, **337**, 713.

[3] J. L. Shi, *Chem. Rev*., 2013, 113, 2139.

[4] S. S. Shendage, U. B. Patil, J. M. Nagarkar, *Tetrahed. Lett.,* **2013**, *54*, 3457-3461.

[5] K. Karami, M. Ghasemi, N. Haghighat Naeini, *Catal. Commun.,* **2013**, *38*, 10-15.

[6] W. Li, B. Zhang, X. Li, H. Zhang, Q. Zhang, *Appl. Catal. A- Gen.,* **2013**, *459*, 65-72.

[7] H.-b. Wang, Y.-h. Zhang, H.-l. Yang, Z.-y. Ma, F.-w. Zhang, J. Sun, J.-t. Ma, *Micropor. Mesopor. Mater.,* **2013**, *168*, 65-72.

[8] P. Wang, F. W. Zhang, Y. Long, M. Xie, R. Li, J. T. Ma, *Catal. Sci. Technol.,* **2013**, *3*, 1618-1624.

[9] B. Cornelio, G. A. Rance, M. Laronze-Cochard, A. Fontana, J. Sapi, A. N. Khlobystov, *J. Mater. Chem., A* **2013**, *1*, 8737-8744.

[10] S. Li, W. Zhang, M.-H. So, C.-M. Che, R. Wang, R. Chen, *J. Mol. Catal. A: Chem.,* **2012**, *359*, 81-87.

[11] R. Li, P. Zhang, Y. Huang, P. Zhang, H. Zhong, Q. Chen, *J. Mater. Chem.,* **2012**, *22*, 22750.

[12] M. Zhu, G. Diao, *J. Phys. Chem. C,* **2011**, *115*, 24743-24749.

[13] Y. Huang, Z. Zheng, T. Liu, J. Lü, Z. Lin, H. Li, R. Cao, *Catal. Commun.,* **2011**, *14*, 27-31.

[14] S. Singha, M. Sahoo, K. M. Parida, *Dalton Trans.* **2011**, *40*, 7130-7132.

[15] P. Dutta, A. Sarkar, *Adv. Synth. Catal.,* **2011**, *353*, 2814-2822.

[16] M. A. Khalily, O. Ustahuseyin, R. Garifullin, R. Genc, M. O. Guler, *Chem. Commun.,* **2012**, *48*, 11358-11360.

[17] Z. Gao, Y. Feng, F. Cui, Z. Hua, J. Zhou, Y. Zhu, J. Shi, *J. Mol. Catal. A: Chem.,* **2011**, *336*, 51-57.

[18] K. M. Deshmukh, Z. S. Qureshi, K. D. Bhatte, K. A. Venkatesan, T. G. Srinivasan, P. R. V. Rao, B. M. Bhanage, *New J. Chem.,* **2011**, *35*, 2747-2751.

[19] Y. Jang, J. Chung, S. Kim, S. W. Jun, B. H. Kim, D. W. Lee, B. M. Kim, T. Hyeon, *Phys. Chem. Chem. Phys.* **2011**, *13*, 2512-2516.

[20] Y. Li, X. Fan, J. Qi, J. Ji, S. Wang, G. Zhang, F. Zhang, *Nano Res.,* **2010**, *3*, 429-437.

[21] B. Tamami, S. Ghasemi, *J. Mol. Catal. A: Chem.,* **2010**, *322*, 98-105.

[22] S. A. Zhou, M. Johnson, J. G. C. Veinot, *Chem. Commun.,* **2010**, *46*, 2411-2413.

[23] J. D. Senra, L. F. B. Malta, M. E. H. M. da Costa, R. C. Michel, L. C. S. Aguiar, A. B. C. Simas, O. A. C. Antunes, *Adv. Synth. Catal.,* **2009**, *351*, 2411-2422.

[24] S. Jana, S. Haldar, S. Koner, *Tetrahed. Lett.,* **2009**, *50*, 4820-4823.

[25] F. Wen, W. Q. Zhang, G. W. Wei, Y. Wang, J. Z. Zhang, M. C. Zhang, L. Q. Shi, *Chem. Mater.,* **2008**, *20*, 2144-2150.

[26] Y. H. Chen, H. H. Hung, M. H. Huang, *J. Am. Chem. Soc.,* **2009**, *131*, 9114-9121.

[27] X. C. Chen, Y. Q. Hou, H. Wang, Y. Cao, J. H. He, *J. Phys. Chem. C,* **2008**, *112*, 8172-8176.

[28] N. Karousis, G. E. Tsotsou, F. Evangelista, P. Rudolf, N. Ragoussis, N. Tagmatarchis, *J. Phys. Chem. C,* **2008**, *112*, 13463-13469.